

# Scintillation Effects in S-Band Telemetry Link of INPE's Earth Station in Cuiabá-Brazil

Antonio Macilio P. de LUCENA<sup>1,2</sup>, Francisco de A. Tavares F. da SILVA<sup>1</sup>, Adeildo S. da SILVA<sup>3</sup>

<sup>1</sup> National Institute for Space Research (INPE), Eusébio, Ceará, Brazil

<sup>2</sup> Fortaleza University (UNIFOR), Fortaleza, Ceará, Brazil

<sup>3</sup> Mackenzie Presbyterian Institute (IPM), CRAAM, ROEN, Eusébio, Ceará, Brazil

antonio.lucena@inpe.br, francisco.silva@inpe.br

Submitted April 29, 2021 / Accepted November 11, 2021

**Abstract.** One of the main earth stations that INPE uses to track and control its satellites is located in the city of Cuiabá (15.33°S, 56.46°W, dip latitude, 6.1°S), between the magnetic equator and the peak of the equatorial anomaly. Based on the GISM model, it is determined that the ionospheric scintillation index ( $S_4$ ) for the telemetry link in the S band (2 208 MHz) between Cuiabá station and the SCD2 satellite, depending on the date and time, can reach values greater than 0.8. This is the first study conducted on ionospheric S-band scintillation in this region of the earth. In this article, the channel model for the link and the telemetry receiver architecture are presented, in order to evaluate subsequently some of ionospheric scintillation effects on the functioning of the communication system. The modulation used is OQPSK and a fully-digital demodulator recovers the carrier phase using a Costas loop and synchronizes the symbols using a Gardner synchronizer. The design of OQPSK demodulator is detailed and the impact of ionospheric scintillation on general demodulator performance and on the functioning of its modules is discussed. The system bit error rate, the error variances of the carrier phase and symbol delay in different conditions of severity of ionospheric scintillation were figured out through computer simulation. From the presented results, it is evident that, for the adopted receiver architecture, which was designed for a space channel without scintillation, there is a substantial degradation on performance of the system even for  $S_4 = 0.5$  and, for the scenario where  $S_4 = 0.8$ , the link becomes practically inoperative.

## Keywords

Equatorial scintillation, S-band space link, OQPSK demodulator, telemetry, satellite communications

## 1. Introduction

Irregularities in the density of electrons in the ionosphere affect the propagation of electromagnetic waves in the space communication links and can cause rapid fluctuations

in the amplitude and phase of the received signal. This phenomenon is called ionospheric scintillation, significantly impairs communications in the VHF and UHF bands, and is more intense in the regions around the magnetic equator and in the auroral / polar zones [1–3].

Low latitude scintillation is called equatorial scintillation and is completely different in terms of the generation mechanism, intensity and statistics from high latitude scintillation [4], [5]. This type of scintillation depends on the frequency of the signal, the season, the solar cycle and usually happens after sunset. In geographic terms, its intensity increases with increasing latitude, measured from the magnetic equator, and it has maximum intensity at points corresponding to the peak of the equatorial anomaly [6].

Brazil is one of the most susceptible countries to equatorial scintillation because its territory extends along the magnetic equator [7]. The main earth station that INPE (National Institute for Space Research) uses to track and control its satellites is located in the city of Cuiabá (15.33°S, 56.46°W, dip latitude, 6.1°S), in the midwest region of Brazil, between the magnetic equator and the peak of the equatorial anomaly.

The papers [6–8] have demonstrated the frequent occurrence of equatorial scintillation at Cuiabá area for the L band, specifically in the operating frequencies of the GNSS systems. Therefore, due to the proximity of the L band (1–2 GHz) to the S band (2–4 GHz), it is reasonable to assume that there is also some degree of scintillation in this spectral band. However, there are no studies that present scintillation intensity measurements for the S band in this region, despite the INPE station in Cuiabá using the frequencies of 2 033 MHz and 2 208 MHz for uplink and downlink, respectively, in the service telecommunication links (telemetry, tracking and command) [9].

It is well known in the literature that ionospheric scintillation degrades the performance of spatial links in the VHF and UHF bands [3, 10–12]. Distortions caused by scintillation in the amplitude and phase of the received signal deteriorates the synchronization of the receivers in addition to having a direct effect on the bit error rate of the systems.

For equatorial scintillation, the impact of amplitude distortion on the functioning of the receiver is usually greater than the one caused by phase distortion [11]. The resulting attenuation in the received signal, in case of great scintillation severity, can be greater than 30 dB, which may result in the complete interruption of the link [3].

The effects of ionospheric scintillation on the functioning of GNSS system receivers have been extensively studied in recent years [3, 13–17] and several techniques to mitigate these effects have been proposed, such as those described in references [18–20], among others. However, the literature is not abundant in studies on the ionospheric scintillation effects in applications involving transionospheric links that are intended for services other than GNSS systems. The impacts of ionospheric scintillation on the performance of some telecommunications systems can be found in the articles [10, 15–17, 21–24] but there is none specific to telemetry communication in S-band.

The central motivation of this research is to investigate the ionospheric scintillation intensity in the S-band telemetry link of the Cuiabá station in Brazil and to evaluate the impacts of this phenomenon on the receiver station functioning and performance. It is assumed that this link uses OQPSK (Offset Quadrature Phase Shift Keying) modulation with baseband pulse formatting [25], bit rate of 10 Mbps, following the recommendations of the Consultative Committee for Space Data System (CCSDS) [26]. From the architecture of the OQPSK demodulator, that was designed for space channel without scintillation, the bit error rate, the performance of the carrier phase recovery and the symbol synchronizer are determined for different scintillation intensity scenarios.

Due to the lack of real measurements of the scintillation intensity in the downlink frequency of the Cuiabá station (2 208 MHz), the GISM model (Global Ionospheric Scintillation Model) [27] was used to make estimates of parameter  $S_4$ , which is normally used to define the scintillation intensity in terms of amplitude. Different orbits for the satellite of interest and several different conditions of solar flux were considered in this estimate.

The main contributions of this work are the estimation of the scintillation intensity ( $S_4$ ) for a S-band link at the Cuiabá-Brazil station in a specific condition of solar activity, the detailing of the architecture and operation of the OQPSK demodulator used in the link and the determination of the demodulator performance in terms of symbol synchronization, carrier recovery and bit error rate for some scintillation intensity scenarios.

This work is organized as follows: in Sec. 2, the channel model is presented, including the statistical description of the scintillation effects on the received signal. The methodology used to estimate  $S_4$  at Cuiabá station for the satellite of interest is described in Sec. 3. In Sec. 4, the architecture of the receiver used in the telemetry link is detailed. The results of the computer simulations to verify the performance

of the system with different degrees of scintillation intensity are presented and discussed in Sec. 5. In Sec. 6, the article is concluded.

## 2. Channel Model

The effect of scintillation on the OQPSK modulated carrier at the symbol rate of  $1/T = 5$  Msps can be modeled as a flat fading whose magnitude follows the Rice distribution [28]. Assuming that  $s_I(t)$  represents the transmitted baseband signal, the received baseband signal is given by

$$r_I(t) = a(t)e^{j\theta(t)}c(t)s_I(t - \tau) + n_I(t) \quad (1)$$

where,  $a(t)$  indicates the attenuation in free space,  $\theta(t)$  corresponds to the phase and frequency offset, including the Doppler shift, and  $\tau$  is the delay due to propagation. The scintillation effect is modeled by  $c(t)$ , while  $n_I(t)$  describes thermal noise, a white, complex white Gaussian process, with zero mean and power spectral density equals to  $N_0$ .

The signal  $c(t)$  is a complex colored Gaussian stochastic process, with a non-zero mean that can be expressed by [28]

$$c(t) = Ae^{\phi} + d(t) \quad (2)$$

where  $A$  is a constant proportional to the amplitude of the part of the signal that reaches the receiver directly through the line of sight (specular component),  $\phi$  is a random variable uniformly distributed between  $-\pi$  and  $+\pi$  and  $d(t)$  is a complex Gaussian process, null mean and variance  $2\sigma^2$ , associated with the part of the signal that undergoes dispersion (multipath component) until it reaches the receiver. Assuming the conservation of power of the transmitted signal, we have

$$E\{|c(t)|^2\} = A^2 + 2\sigma^2 = 1 \quad (3)$$

where  $E\{x\}$  is the statistical average of  $x$ . Since the angular distribution of the scattered signal is approximately Gaussian for circular antennas [29], the autocorrelation function of the process  $d(t)$  is given by

$$R_d(\tau) = E\{d(t)d^*(t + \tau)\} = 2\sigma^2e^{-(\tau/\tau_0)^2} \quad (4)$$

where the asterisk indicates the complex conjugate operation and  $\tau_0$  is the decorrelation time. The value of  $\tau_0$  depends on the frequency of the signal and, for equatorial scintillation during the night, it can be determined by the expression [29]:

$$\tau_0 = 0.1f/250 \quad (5)$$

where  $f$  is the signal frequency in MHz. For the case under study,  $f = 2\,208$  MHz, and  $\tau_0 \cong 0.883$  s is obtained.

The magnitude of  $c(t)$ , denoted by  $\alpha = |c(t)|$ , follows the Rice distribution and its probability density function is expressed by [28]

$$p_\alpha(\alpha) = 2\alpha(1 + K)e^{-K - \alpha^2(1+K)}I_0\left[2\alpha\sqrt{K(1+K)}\right] \quad (6)$$

where  $K = A^2/2\sigma^2$  is the Rician parameter and  $I_0[\cdot]$  is the modified Bessel function of the first type and zero order.

The scintillation index  $S_4$  is defined by [12]

$$S_4 = \sqrt{\frac{\langle I^2 \rangle - \langle I \rangle^2}{\langle I \rangle^2}} \quad (7)$$

where  $I = \alpha^2$  and the operator  $\langle \cdot \rangle$  is the mean over the time. The Rician  $K$  parameter is related to the scintillation index  $S_4$  by the following equation [30]:

$$K = \sqrt{1 - S_4^2} / \left( 1 - \sqrt{1 - S_4^2} \right). \quad (8)$$

The model for generating  $c[i]$ , the discrete version of process  $c(t)$ , used in the numerical simulations of this work, is represented in Fig. 1. Noise generator blocks I and II produce sequences of white Gaussian noise samples, independent of each other, with zero mean and variance equal to 0.5. The output of the Noise generator II is multiplied by  $j = \sqrt{-1}$  in order to obtain samples of white and complex Gaussian noise with zero mean and unit variance. This new noise is filtered by the Gaussian filter (unit power gain) and then multiplied by the constant  $k_1 = \sqrt{2}\sigma$ , resulting in the stochastic process  $d[i]$  which corresponds to the discretized process  $d(t)$ . The process autocorrelation function follows a Gaussian function, described by (4), with a correlation time equals to  $\tau_0 = 0.883$  s. Finally, the constant  $Ae^{j\phi}$  is added to the samples of  $d[i]$ , related to the specular component of the signal, as described in (2), resulting in process  $c[i]$ .

The Gaussian filter is implemented by a discrete FIR filter with an impulsive response containing 256 taps, determined from the equations presented in [28]. The sampling frequency used in this generator is equal to 50 Hz.

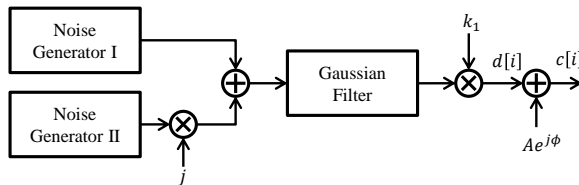


Fig. 1. Model for generating scintillation effects.

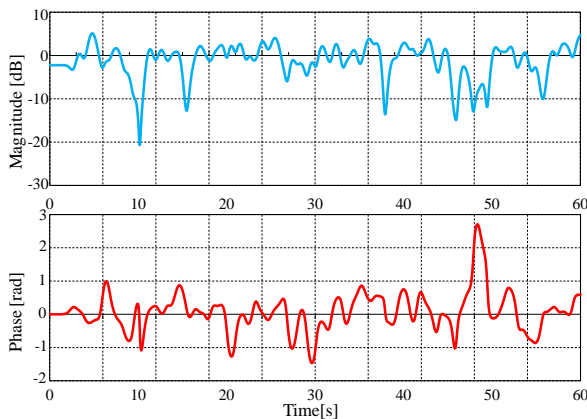


Fig. 2. Magnitude and phase of  $c[i]$  for  $S_4 = 0.8$ .

The generator setting is made as follows: a- first, define the value of  $S_4$ ; b- using (8),  $K$  is determined; c- the constant  $k_1$  is given by  $k_1 = \sqrt{2}\sigma = \sqrt{1/(1+K)}$ ; d- the specular component is calculated by  $A = \sqrt{2\sigma^2 K}$  with  $\phi = 0$ .

Figure 2 shows the magnitude and phase of  $c[i]$  for a period of 60 s and are determined by the model described in Fig. 1 in the condition of  $S_4 = 0.8$ .

### 3. Estimate of Index $S_4$ in Cuiabá

The methodology developed for the estimation of  $S_4$  uses the ionospheric scintillation model GISM (Global Ionospheric Scintillation Model) [31], [32] that is adjusted with the parameters of the orbital mechanics obtained from the satellite tracker software called N2YO [33]. Several other data related to the satellite-earth station link also feed the GISM.

The GISM model is recommended by the International Telecommunication Union (ITU) [34] and allows the determination of  $S_4$ , among other scintillation parameters, as detailed by [32]. The model needs some specific entries such as: a-location of the receiving station; b-satellite orbit parameters; c-frequency of the carrier link; d-year, month and hour and e-solar flow. Once the inputs are inserted, the GISM model determines the scintillation index  $S_4$ , treating the ionosphere as a turbulent multilayered medium, each one acting as a phase screen. The electronic density of the medium is provided by the empirical model of ionospheric electronic density named NeQuick [35].

The satellite considered for this estimate of  $S_4$  is the Brazilian satellite for collecting environmental data, called SCD2 (NORAD ID: 25504), developed by INPE, whose orbital parameters are: a- perigee: 739.8 km; b- apogee: 764.3 km; c- inclination: 25.0°; and d- period: 99.7 minutes. The adopted average altitude of the satellite is 750 km. The earth station of link is the INPE's station located at Cuiabá (Latitude: 15°33'S; Longitude: 56°04'W). In the estimates, the downlink frequency is 2 208 MHz and the observations are restricted to elevation angle greater than 25.0°.

In order to determine  $S_4$ , three passages from the SCD2 satellite were selected, occurring on October 16, 17 and 19 of the year 2014. The year 2014 has already been analyzed in other studies that describe the effects of scintillation on GNSS receivers [8], [36]. It is noteworthy that the solar maximum of the 11-year solar cycle had already occurred in 2013 and, therefore, this analysis in 2014 is not the worst case. The solar flux on the investigated days is less than 170 sfu (1 sfu =  $10^4$  Jy), which does not represent an extreme solar activity. Consequently, the values of  $S_4$  estimated in this work for the frequency of 2 208 MHz do not represent the most severe scintillation condition for the Cuiabá station.



Fig. 3. Tracing the SCD2 orbit with respect to Cuiabá.

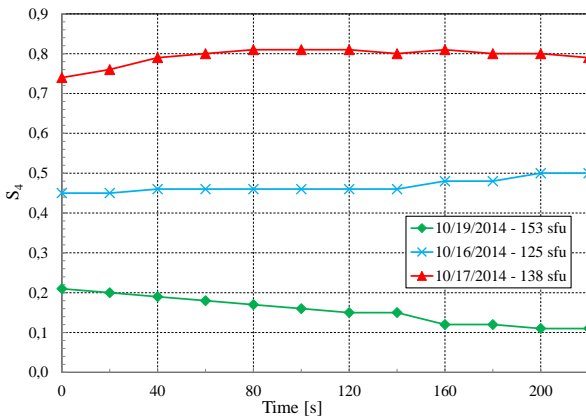


Fig. 4. Obtained  $S_4$  by GISM for three SCD2 passages through Cuiabá.

The same orbit was assumed for all satellite passages. Figure 3 illustrates the SCD2 orbit with respect to Cuiabá station and the magnetic equator. The light gray curve corresponds to the satellite orbit, the receiving station is indicated by the black point and the magnetic equator is the curve drawn in the dark gray.

The values of  $S_4$  are determined every 20 s during the passage of the satellite. Figure 4 presents the values of  $S_4$  as a function of time obtained by GISM when simulating SCD2 passages that took place on 10/19/2014 at 3:00 LT, 10/16/2014 at 21:00 LT and 10/17/2014 at 23:00 LT, respectively. The results presented in Fig. 4 show a wide variability in the intensity of the scintillation, expressed by the  $S_4$  values. The minimum and maximum observed values are about  $S_4 = 0.1$  on day 19 and  $S_4 = 0.8$  on day 17, respectively.

### 4. Receiver Architecture

Figure 5 shows the simplified block diagram of the earth station receiver. The RF signal in the S band is received by the antenna, then amplified and converted to an intermediate frequency (IF) of 70 MHz by the RF front-end block. The A/D converter performs the analog-to-digital conversion with the sampling frequency  $f_s = 8/T = 40$  MHz, deriving

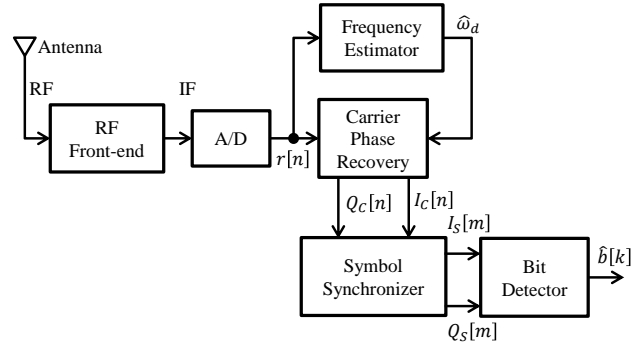


Fig. 5. Earth station OQPSK receiver block diagram.

the discrete signal  $r[n]$  expressed by

$$r[n] = I[n] \cos \{(\omega_{IF} + \omega_d)n + \varphi[n]\} - Q[n] \sin \{(\omega_{IF} + \omega_d)n + \varphi[n]\} + w[n] \tag{9}$$

where  $I[n]$  and  $Q[n]$  are the in-phase and quadrature components of the discrete signal, respectively,  $\omega_{IF}$  is the discrete frequency corresponding to 70 MHz IF,  $\omega_d$  represents the frequency offset with respect to the nominal frequency  $\omega_{IF}$  and  $\varphi[n]$  indicates the carrier phase fluctuation, including the scintillation effect. Discrete Gaussian white noise with zero mean and variance  $N_0 f_s / 2$  is represented by  $w[n]$ . From that point on, all signal processing of the receiver is done in the discrete domain.

Initially, the frequency estimator block estimates the frequency offset ( $\omega_d$ ) and passes the estimated value ( $\hat{\omega}_d$ ) on to the carrier phase recovery block. This block, in turn, generates a replica of the received carrier, synchronized in frequency and phase, and from  $r[n]$ , it derives a version of the in-phase and quadrature components of the received signal, denoted by  $I_c[n]$  and  $Q_c[n]$ . The symbol synchronizer block interpolates and decimates the  $I_c[n]$  and  $Q_c[n]$  signals to obtain the  $I_s[m]$  and  $Q_s[m]$  signals that correspond, for each instant, to the maximum magnitude sample associated with the received symbol. The last block shown in Fig. 5, bit detector, utilizes samples  $I_s[m]$  and  $Q_s[m]$  for the detection of received symbols and their conversion into the bit sequence indicated by the signal  $\hat{b}[k]$ .

Figure 6 illustrates the block diagram of the carrier phase recovery. The adopted solution is a second order directed-decision Costas loop, already very well studied in the literature [37]. The input signal  $r[n]$  is multiplied by the recovered carrier and the resulting signals are filtered in arms  $I$  and  $Q$  of the loop by the low pass filters of impulsive response  $g_m[n]$ . These filters are of the type of the raised cosine root with roll-off  $\alpha = 0.5$  and are matched to the formatting pulse of the transmitted signal. The signals  $I_c[n]$  and  $Q_c[n]$  are used to detect the bits and to determine the phase error signal  $e[n]$ . The estimated phase  $\hat{\varphi}[n]$ , resulting from the passage of  $e[n]$  through the discrete filter, is input from the LUT (Look-up table) that generates the two versions of the carrier (cosine and sine) for loop feedback.

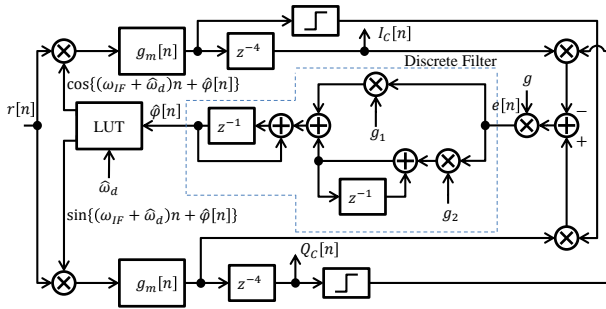


Fig. 6. Carrier phase recovery block diagram.

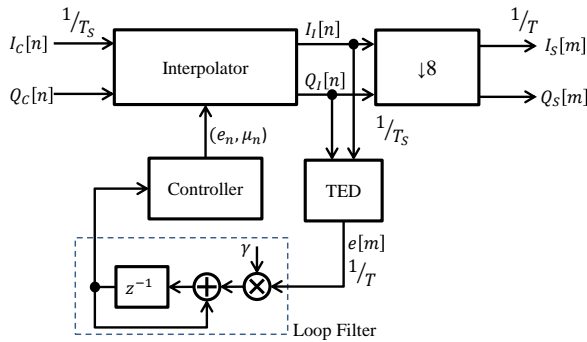


Fig. 7. Symbol synchronizer block diagram.

The transfer function of the Costas loop is [37], [38]

$$H(z) = \frac{(g_1 + g_2)z - g_1}{z^2 + (g_1 + g_2 - 2)z + (1 - g_1)} \quad (10)$$

where  $g_1$  and  $g_2$ , as shown in Fig. 6, are associated with the loop filter. In this case, the noise bandwidth ( $B_L T_s$ ) of  $H(z)$  is defined by [38]

$$2B_L T_s = \frac{1}{2\pi j} \oint H(z)H(z^{-1})z^{-1} dz = \frac{(b_1^2 + b_2^2)(1 + a_2) - 2b_1 b_2 a_1}{(1 - a_2) [(1 + a_2)^2 - a_1^2]} \quad (11)$$

where  $T_s$  is the sampling period,  $a_1 = g_1 + g_2 - 2$ ,  $a_2 = 1 - g_1$ ,  $b_1 = g_1 + g_2$  and  $b_2 = -g_1$ . In this project,  $B_L T_s = 2.5 \times 10^{-4}$  was adopted.

The symbol synchronizer used in this receiver implements the Gardner synchronizer [37], [39] and its block diagram is shown in Fig. 7. The  $I_c[n]$  and  $Q_c[n]$  signals, corresponding to the filtered and asynchronous samples of the baseband signal, taken at  $t = nT_s$ , are delivered to the interpolator. This one, in turn, makes the necessary interpolation to produce the samples  $I_1[n]$  and  $Q_1[n]$ , at times  $t = (l_n + \mu_n)T_s$ , where  $l_n$  and  $\mu_n$  are the base point index and the fractional interval respectively, both determined by the controller block. The decimated samples  $I_s[m]$  and  $Q_s[m]$ , output from the downsampling block, at the symbol rate ( $1/T$ ), are delivered to bit detector for information retrieval. The TED (Time error detector) block also receives the  $I_1[n]$  and  $Q_1[n]$  signals to derive the error signal  $e[m]$  which, after being filtered through the loop filter, serves as

an input to the Controller block. The constant  $\gamma$  indicates the filter adaptation step.

This synchronizer can be modeled as a first order closed loop with the following transfer function [37]:

$$F(z) = \frac{k_d \gamma z^{-1}}{1 + (k_d \gamma - 1) z^{-1}} \quad (12)$$

where  $k_d$  is the gain of TED. The noise bandwidth ( $B_n T$ ) of  $F(z)$  is given by [37]:

$$B_n T = \frac{k_d \gamma}{2(2 - k_d \gamma)}. \quad (13)$$

Therefore, choosing  $B_n T = 2.51 \times 10^{-3}$  results in  $k_d \gamma = 0.01$ .

## 5. Numerical Results and Discussions

In this section, some performance results of the OQPSK demodulator, obtained through computer simulation, are presented and discussed. The error variances of the recovered phase and estimated delay and also the bit error rate under different scintillation severity conditions were evaluated.

Figure 8 describes the model of the simulated system, defining the input and output parameters. The received signal equation  $r[n]$ , shown in the figure, is derived from (9), by replacing  $\omega_{IF} + \omega_d$  with  $\omega_c$ , which is the discrete frequency of the carrier. The system model is implemented in Simulink running in a computer with Windows operational system.

The main parameters used in the model are described in Tab. 1. Its values reflect the operating conditions of the system. It is interesting to note that in this model the carrier frequency and bit rate were reduced by a factor of 1000 in relation to the actual values. This reduction is possible because the parameters to be evaluated in this study, the error variances of the phase and delay estimators and the bit error rate, only depend on the bandwidth of the loops, expressed by  $B_L T_s$  and  $B_n T$ ,  $E_b/N_0$  and  $S_4$  which are chosen with the same values as the station's OQPSK demodulator. This decrease in frequency allows the computer simulation of the system to be accelerated. Using a computer with a 1.7 GHz Intel Core i5, the time needed to simulate the demodulation of the received signal over a period of 60 s is approximately 65 s.

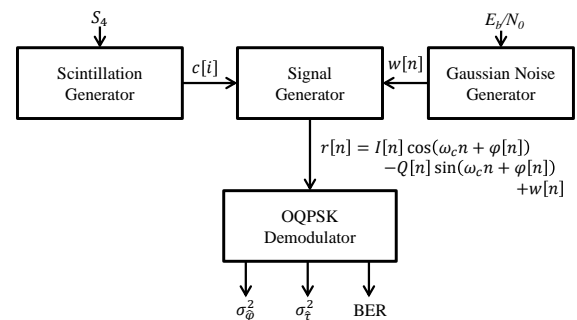


Fig. 8. Model of the system used in the simulations.

Parameter	Value
Frequency of the subcarrier ( $f_c$ )	70 kHz
Bit rate ( $2/T$ )	10 kbps
Sampling frequency ( $f_s$ )	40 kHz
Noise bandwidth of Costa loop ( $B_L T_s$ )	$2.50 \times 10^{-4}$
Noise bandwidth of the symbol synchronizer loop ( $B_n T$ )	$2.51 \times 10^{-3}$
Bit energy per noise density ( $E_b/N_0$ )	$0 \text{ dB} \leq E_b/N_0 \leq 20 \text{ dB}$
Decorrelation time	0.883

Tab. 1. Model parameters used in the simulation.

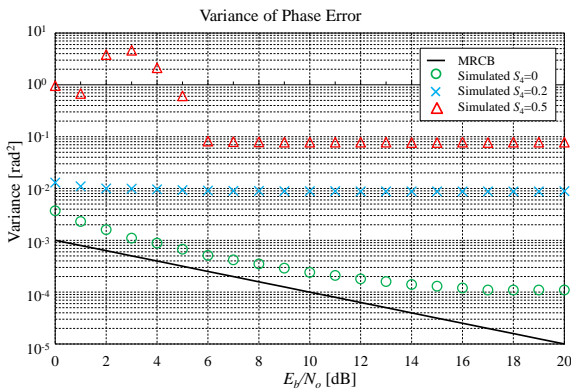


Fig. 9. Curves of the variance of the phase error of the recovered carrier.

The simulated phase error variance of the recovered carrier ( $\sigma_{\varphi}^2$ ) as a function of  $E_b/N_0$ , and parameterized by  $S_4 = 0.0$  (without scintillation),  $S_4 = 0.2$  and  $S_4 = 0.5$ , are shown in Fig. 9. As a reference, the modified Cramer-Rao bound (MCRB) curve for this variance is also presented and given by the following equation [37]:

$$\text{MCRB}(\varphi) = \frac{B_L T}{2E_b/N_0}. \tag{14}$$

It is evident from the results shown in Fig. 9 that, without scintillation,  $\sigma_{\varphi}^2$  approaches  $\text{MCRB}(\varphi)$  for  $E_b/N_0 < 10 \text{ dB}$ , as predicted in the literature [37]. It is also noticed that for  $S_4 = 0.2$  there is an increase in the values of  $\sigma_{\varphi}^2$ , with respect to the case without scintillation, for the whole range of  $E_b/N_0$  tested. In this case, the curve is practically constant from  $E_b/N_0 > 5 \text{ dB}$ , indicating that the contribution of Gaussian noise is insignificant in relation to the scintillation effect. In this condition of  $S_4$ , the phase recovery loop works without loss of lock or cycle slip occurrence, for the entire  $E_b/N_0$  interval, which is evidenced by the smoothness of the  $\sigma_{\varphi}^2$  curve.

The results for  $S_4 = 0.5$  shows that values of  $\sigma_{\varphi}^2$  are much higher than the values observed for  $S_4 = 0.2$ . For  $E_b/N_0 > 5 \text{ dB}$ , the variance is almost constant because in this condition the effect of Gaussian noise in  $\sigma_{\varphi}^2$  is negligible. It is also observed that for  $E_b/N_0 \leq 5 \text{ dB}$  the points are outside the curve, with extremely high values of variance. This indicates the occurrence of loss of lock and/or cycle slip in the Costas loop. Figure 10 illustrates this phenomenon,

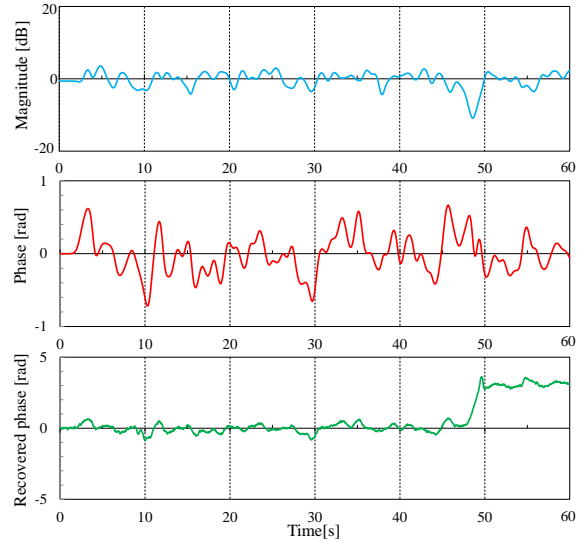


Fig. 10. Recovered phase showing the occurrence of cycle slip.

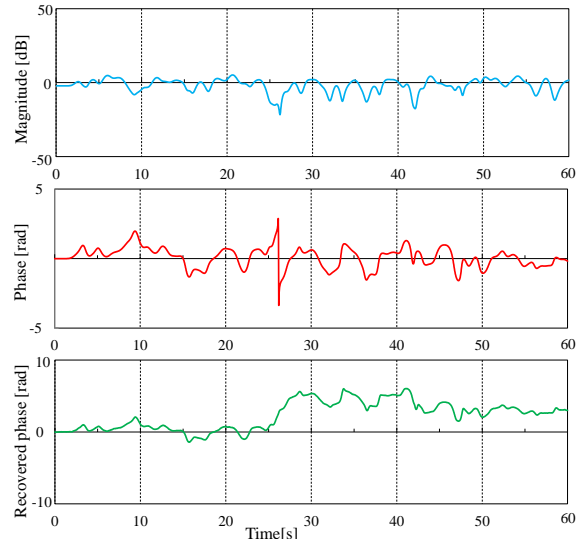


Fig. 11. Recovered phase for  $S_4 = 0.8$  and  $E_b/N_0 = 50 \text{ dB}$ .

showing the phase recovered in a simulation period of 60 s,  $E_b/N_0 = 2 \text{ dB}$  and  $S_4 = 0.5$ , together with the amplitude and phase curves of the scintillation process  $c[i]$ . There is a cycle slip with a phase jump equal to  $\pi$  at an instant close to 50 s. It is interesting to notice that the recovered phase is identical to the scintillation phase, both before and after the cycle slip, showing that the Costas loop was and remained in lock. In the measurements made, when  $E_b/N_0 > 5 \text{ dB}$ , there was no cycle slip, indicating that, for  $S_4 = 0.5$ , the increase in  $E_b/N_0$  prevents the occurrence of this problem.

Performed simulations with  $S_4 = 0.8$  showed that the increase in  $E_b/N_0$  is no longer effective as a technique for mitigating cycle slip and /or loss of lock. In all simulations made with  $S_4 = 0.8$ , for a period of 60 s, there was a cycle slip and/or loss of lock, even for  $E_b/N_0 = 50 \text{ dB}$ . Figure 11 shows the amplitude and phase of the process  $c[i]$  and also the recovered phase for  $S_4 = 0.8$  and  $E_b/N_0 = 50 \text{ dB}$ . It is observed that a cycle slip occurred in about 26 s, probably due to the sudden variation of the scintillation phase.

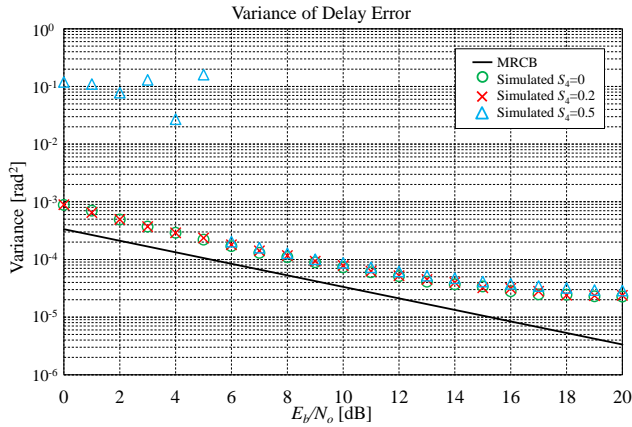


Fig. 12. Symbol delay error variance curves.

Curves of the normalized variance of the symbol delay error, indicated by  $\sigma_{\hat{\tau}}^2$ , as a function of  $E_b/N_0$ , without scintillation and with scintillation ( $S_4 = 0.8$  and  $0.5$ ), are shown in Fig. 12. The normalized modified Cramer-Rao bound  $MCRB(\tau)$ , given by (15) [40], where  $\alpha$  is the roll-off of the baseband pulse formatter, is also plotted in Fig. 12.

$$MCRB(\tau) = \frac{B_n T}{2[\pi^2(1 + \alpha^2)/3 - 8\alpha^2](E_b/N_0)}. \quad (15)$$

From the results of Fig. 12, it can be seen that, except for the points where the cycle slip occurs ( $E_b/N_0 \leq 5$  dB, for  $S_4 = 0.5$ ) in the Costas loop, the scintillation affects very little performance of the symbol timing synchronizer. If there is a cycle slip in the carrier phase recovery, the Gardner synchronizer also loses the lock, resulting in excessive measurements of  $\sigma_{\hat{\tau}}^2$ . This characteristic stems from the demodulator’s architecture, in which the symbol synchronization takes place after the conversion to baseband that needs carrier phase recovery. Therefore, cycle slip events in the Costa loop also cause loss of synchronization in symbol recovery. Figure 13 illustrates the symbol delay and the carrier phase recovered by demodulator in the condition where the symbol delay is  $T/2$ ,  $E_b/N_0 = 5$  dB and  $S_4 = 0.5$ . We observe a cycle slip event around 50 s and the consequent loss of symbol synchronization.

Figure 14 illustrates the demodulator’s bit error rate (BER), determined under three different operating conditions (no scintillation,  $S_4 = 0.2$  and  $0.5$ ) and compared with the theoretical BER curve for an OQPSK system with optimum detection. Without scintillation, the system’s BER is practically similar to the theoretical limit. When  $S_4 = 0.2$  and  $S_4 = 0.5$ , there are degradations of approximately 1 dB and 7 dB, respectively, in the condition of  $BER = 10^{-5}$ . The BER equal to  $10^{-5}$  is the maximum value specified for the system operation. These estimated losses by simulation are consistent with the performance of systems described in literature [10], [41]. In these case, the communication channel is modeled as a Rician channel.

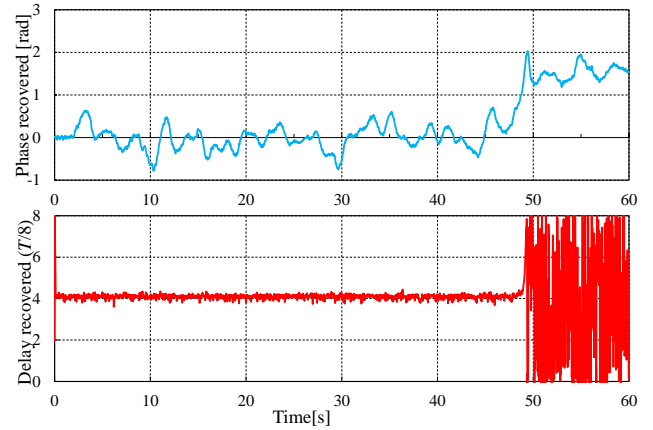


Fig. 13. Recovered phase and delay for  $E_b/N_0 = 5$  dB and  $S_4 = 0.5$ .

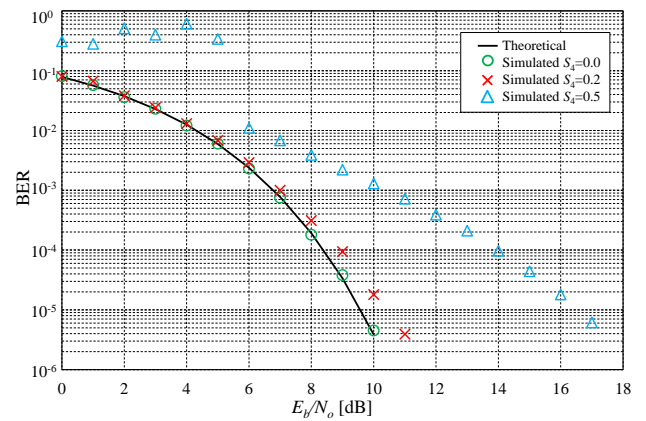


Fig. 14. BER curves of the OQPSK demodulator.

The points outside the curve when  $S_4 = 0.5$  and  $E_b/N_0 \leq 5$  dB reveal the demodulator’s loss of synchronization caused by the cycle slip as previously mentioned. It is noteworthy that in the condition of great scintillation severity ( $S_4 = 0.8$ , for example) increasing the value of  $E_b/N_0$ , even if it is by a factor of 1000 (30 dB), does not prevent the occurrence of cycle slip and, for consequence, there is an exaggerated increase in BER. Some strategies to mitigate this problem are still the subject of our studies.

## 6. Conclusions

In this work, using the GISM model, we show the occurrence of ionospheric scintillation in the S band link (2 208 MHz) between the INPE earth station in Cuiabá and the SCD2 satellite. Assuming the solar flow of October 2014, we find scintillation indices as high as  $S_4 = 0.8$ . Therefore, it becomes evident that this communication link can be subjected to severe conditions of ionospheric scintillation.

We present the channel model and architecture of the receiver to study the impact of scintillation on system performance in the tracking phase. The station’s OQPSK demodulator uses a Costas loop for carrier phase recovery and a closed loop with Gardner detector for symbol synchronization.

The results of the computer simulation show that, without scintillation, the bit error rate of OQPSK demodulator is close to the theoretical limit and the error variances of carrier phase and of symbol delay are in accordance with the performances presented in the literature.

The carrier phase recovery is much more susceptible to the effects of scintillation than the symbol synchronizer. Even for low severity scintillation ( $S_4 = 0.2$ ), there is a large increase in the estimated phase variance compared to the null scintillation condition. On the other hand, the performance of the symbol synchronizer is practically identical for  $S_4 = 0.0$  and  $S_4 = 0.2$ .

When  $S_4 = 0.5$  and  $E_b/N_0 \leq 5$  dB, the occurrence of cycle slips is observed in the Costas loop, during the simulation periods adopted to determine  $\sigma_{\hat{\phi}}^2$ ,  $\sigma_{\hat{\tau}}^2$  and BER. The loss of lock in the carrier phase recovery, due to the cycle slip, causes also loss of lock in the symbol synchronizer. On the other hand, if  $S_4 = 0.5$  and  $E_b/N_0 > 5$  dB, the symbol synchronizer remains practically immune to scintillation, with the values of  $\sigma_{\hat{\tau}}^2$  close to those obtained for  $S_4 = 0.0$ . In contrast, the carrier phase recovery, under these conditions, experiences an increase in  $\sigma_{\hat{\phi}}^2$  by a factor of ten when compared to the values obtained for  $S_4 = 0.2$ .

Scintillation causes an increase in the bit error rate of the OQPSK demodulator. Comparing the BER curves for  $S_4 = 0.2$  and  $S_4 = 0.5$ , there are losses of 1 dB and 7 dB, respectively, with respect to the case without scintillation, in the condition of  $\text{BER} = 10^{-5}$ .

The results also show that for  $S_4 = 0.8$ , the receiver with the described architecture, due to the occurrence of cycle slip, is unable to maintain the synchronism for a period of 60 s, even when  $E_b/N_0$  is as high as 50 dB.

In summary, we conclude that, for the described OQPSK demodulator, the communication link has substantial loss of performance even for moderate scintillation intensity ( $S_4 = 0.5$ ) and completely deteriorates when  $S_4$  is equal to 0.8.

As a deployment of this work, the study of new techniques is planned to mitigate the effects of ionospheric scintillation in the functioning of the symbol synchronizer and in the carrier recovery module. Measurements at Cuiabá station of the  $S_4$  parameter carried out simultaneously in the L and S band are being organized in order to understand the correlation of the scintillation intensity in these two frequency bands.

## Acknowledgments

We thank the National Institute for Space Research (INPE) and the Mackenzie Presbyterian Institute (IPM) for all support given to this work.

## References

- [1] WHITNEY, H. E., BASU, S. The effect of ionospheric scintillation on VHF/UHF satellite communications. *Radio Science*, 1977, vol. 12, no. 1, p. 123–133. DOI: 10.1029/RS012i001p00123
- [2] IPPOLITO, L. J. *Radiowave Propagation in Satellite Communications*. Springer Science & Business Media, 2012. ISBN: 0442240112
- [3] KINTNER, P. M., LEDVINA, B. M., DE PAULA, E. R. GPS and ionospheric scintillations. *Space Weather*, 2007, vol. 5, no. 9, p. 1–23. DOI: 10.1029/2006SW000260
- [4] BASU, S., MACKENZIE, E.M., BASU, S., et al. 250 MHz/GHz scintillation parameters in the equatorial, polar, and auroral environments. *IEEE Journal on Selected Areas in Communications*, 1987, vol. 5, no. 2, p. 102–115. DOI: 10.1109/JSAC.1987.1146533
- [5] JIAO, Y., MORTON, Y. T., TAYLOR, S., et al. Characterization of high-latitude ionospheric scintillation of GPS signals. *Radio Science*, 2013, vol. 48, no. 6, p. 698–708. DOI: 10.1002/2013RS005259
- [6] DE PAULA, E. R., RODRIGUES, F. S., IYER, K. N., et al. Equatorial anomaly effects on GPS scintillations in Brazil. *Advances in Space Research*, 2013, vol. 31, no. 3, p. 749–754. DOI: 10.1016/S0273-1177(03)00048-6
- [7] AQUINO, M. Coutering Ionospheric Disturbances Affecting GNSS in Brazil. *GPS World*, 2015.
- [8] KOULOURI, A., SMITH, N. D., VANI, B. C., et al. Methodology to estimate ionospheric scintillation risk maps and their contribution to position dilution of precision on the ground. *Journal of Geodesy*, 2020, vol. 94, no. 2, p. 1–22. DOI: 10.1007/s00190-020-01344-0
- [9] DE LUCENA, A. M. P., DA SILVA, A. S., VIOT, D. D., et al. Design of a fully-digital BPSK demodulator integrated into a TT&C transponder. *IEEE Latin America Transactions*, 2020, vol. 18, no. 9, p. 1511–1520. DOI: 10.1109/TLA.2020.9381792
- [10] FERREIRA, P. V. R., WYGLINSKI, A. M. Performance analysis of UHF mobile satellite communication system experiencing ionospheric scintillation and terrestrial multipath fading. In *IEEE Vehicular Technology Conference (VTC2015-Fall)*. Boston (MA, USA), 2015, p. 1–5. DOI: 10.1109/VTCSFall.2015.7391072
- [11] MORAES, A. DE O., PERRELLA, W. J. Performance evaluation of GPS receiver under equatorial scintillation. *Journal of Aerospace Technology and Management*, 2009, vol. 1, no. 2, p. 193–200. DOI: 10.5028/jatm.2009.0102193200
- [12] HUMPHREYS, T. E., PSIAKI, M. L., HINKS, J. C., et al. Simulating ionosphere-induced scintillation for testing GPS receiver phase tracking loops. *IEEE Journal of Selected Topics in Signal Processing*, 2009, vol. 3, no. 4, p. 707–715. DOI: 10.1109/JSTSP.2009.2024130
- [13] KINTNER, P. M., HUMPHREYS, T., HINKS, J. GNSS and ionospheric scintillation. *Inside GNSS*, 2009, vol. 4, no. 4, p. 22–30.
- [14] LINTY, N., FARASIN, A., FAVENZA, A., et al. Detection of GNSS ionospheric scintillations based on machine learning decision tree. *IEEE Transactions on Aerospace and Electronic Systems*, 2018, vol. 55, no. 1, p. 303–317. DOI: 10.1109/TAES.2018.2850385
- [15] VILA-VALLS, J., LINTY, N., CLOSAS P., et al. Survey on signal processing for GNSS under ionospheric scintillation: Detection, monitoring, and mitigation. *NAVIGATION, Journal of the Institute of Navigation*, 2020, vol. 67, no. 3, p. 511–536. DOI: 10.1002/navi.379
- [16] SALLES, L. A., VANI, B. C., MORALES, A., et al. Investigating ionospheric scintillation effects on multifrequency GPS signals. *Surveys in Geophysics*, 2021, vol. 42, p. 999–1025. DOI: 10.1007/s10712-021-09643-7

- [17] PORTELLA, I. P., MORAES A. DE O., PINHO, M. DA S., et al. Examining the tolerance of GNSS receiver phase tracking loop under the effects of severe ionospheric scintillation conditions based on its bandwidth. *Radio Science*, 2021, vol. 56, no. 6, p. 1–11. DOI: 10.1029/2020RS007160
- [18] SIVAVARAPRASAD, G., PADMAJA, R. S., RATNAM, D. V. Mitigation of ionospheric scintillation effects on GNSS signals using variational mode decomposition. *IEEE Geoscience and Remote Sensing Letters*, 2017, vol. 14, no. 3, p. 389–393. DOI: 10.1109/LGRS.2016.2644723
- [19] VILA-VALLS, J., CLOSAS, P., FERNANDEZ-PRADES, C., et al. On the mitigation of ionospheric scintillation in advanced GNSS receivers. *IEEE Transactions on Aerospace and Electronic Systems*, 2018, vol. 54, no. 4, p. 1692–1708. DOI: 10.1109/TAES.2018.2798480
- [20] GUO, K., VEETIL, S. V., WEAVER, B. J., et al. Mitigating high latitude ionospheric scintillation effects on GNSS Precise Point Positioning exploiting 1-s scintillation indices. *Journal of Geodesy*, 2021, vol. 95, no. 3, p. 1–15. DOI: 10.1007/s00190-021-01475-y
- [21] DAVIES, K., SMITH, E. K. Ionospheric effects on satellite land mobile systems. *IEEE Antennas and Propagation Magazine*, 2002, vol. 44, no. 6, p. 24–31. DOI: 10.1109/MAP.2002.1167260
- [22] SUPNITHI, P., WONGTRAIAT, W., TANTARATANA, S. Performance of M-PSK in mobile satellite communication over combined ionospheric scintillation and flat fading channels with MRC diversity. *IEEE Transactions on Wireless Communications*, 2009, vol. 8, no. 7, p. 3360–3364. DOI: 10.1109/TWC.2009.080208
- [23] AJIBOYE, A., ABDULRAHMAN, A. Y., FALADE, A. J., et al. Effects of ionospheric scintillation on communication systems: GPS and satellite. *Telecommunications and Radio Engineering*, 2017, vol. 76, no. 20, p. 1849–1859. DOI: 10.1615/TelecomRadEng.v76.i20.50
- [24] FERNANDEZ, L., RUIZ-DE-AZUA, J. A., CALVERAS, A., et al. Assessing LoRa for satellite-to-earth communications considering the impact of ionospheric scintillation. *IEEE Access*, 2020, vol. 8, p. 165570–165582. DOI: 10.1109/ACCESS.2020.3022433
- [25] SILVA, A. S., LUCENA, A. M. P., MOTA, J. C. M. *Demodulator OQPSK: Fully Digital Implementation for Space Applications (Demodulador OQPSK: Implementação Completamente Digital para Aplicações Espaciais)*. (In Portuguese) Novas Edições Acadêmicas, 2014. ISBN: 9783639692532
- [26] CCSDS. *Recommendations for Space Data System Standards. Bandwidth-efficient Modulations*. CCSDS 413.0-G-1, Green Book, 2003.
- [27] BÉNIGUEL, Y., FORTE, B., RADICELLA, S., et al. Scintillations effects on satellite to earth links for telecommunication and navigation purposes. *Annals of Geophysics*, 2004, vol. 47, no. 2/3, p. 1179–1199. DOI: 10.4401/ag-3293
- [28] YE, Z., SATORIUS, H. Channel modeling and simulation for mobile user objective system (MUOS)—part 1: Flat scintillation and fading. In *IEEE International Conference on Communications (ICC)*. Anchorage (AK, USA), 2003, p. 3503–3510. DOI: 10.1109/ICC.2003.1204106
- [29] KULLSTAM, P. A., KESKINEN, M. J. Ionospheric scintillation effects on UHF satellite communications. In *MILCOM 2000 Proceedings. 21st Century Military Communications. Architectures and Technologies for Information Superiority*. Los Angeles (CA, USA), 2000, p. 779–783. DOI: 10.1109/MILCOM.2000.904036
- [30] SHAFT, P. On the relationship between scintillation index and Rician fading. *IEEE Transactions on Communications*, 1974, vol. 22, no. 5, p. 731–732. DOI: 10.1109/TCOM.1974.1092244
- [31] BÉNIGUEL, Y., BUONOMO, S. A. Multiple phase screen propagation model to estimate fluctuations of transmitted signals. *Physics and Chemistry of the Earth, Part C: Solar, Terrestrial & Planetary Science*, 1999, vol. 24, no. 4, p. 333–338. DOI: 10.1016/S1464-1917(99)00007-0
- [32] BÉNIGUEL, Y. Global ionospheric propagation model (GIM): A propagation model for scintillations of transmitted signals. *Radio Science*, 2002, vol. 37, no. 3, p. 1–13. DOI: 10.1029/2000RS002393
- [33] N2YO. *Real Time Satellite Tracking and Predictions*. [Online] Cited 2021-01-25. Available at <https://www.n2yo.com>
- [34] ITU. *Transionospheric Radio Propagation. The Global Ionospheric Scintillation Model (GISM)*. REPORT ITU-R P.2097, 2007.
- [35] RADICELLA, S. M. The NeQuick model genesis, uses and evolution. *Annals of Geophysics*, 2009, vol. 52, no. 3/4, p. 417–422. DOI: 10.4401/ag-4597
- [36] MORAES, A. O., VANI, B. C., COSTA, E., et al. Ionospheric scintillation fading coefficients for the GPS L1, L2, and L5 frequencies. *Radio Science*, 2018, vol. 53, no. 9, p. 1165–1174. DOI: 10.1029/2018RS006653
- [37] MENGALI, U. *Synchronization Techniques for Digital Receivers*. Springer Science & Business Media, 2013. ISBN: 9781489918079
- [38] LINDSEY, W. C., CHIE, C. M. A survey of digital phase-locked loops. *Proceedings of the IEEE*, 1981, vol. 69, no. 4, p. 410–431. DOI: 10.1109/PROC.1981.11986
- [39] GARDNER, F. M. A BPSK/QPSK timing-error detector for sampled receivers. *IEEE Transactions on Communications*, 1986, vol. 34, no. 5, p. 423–429. DOI: 10.1109/TCOM.1986.1096561
- [40] SHI, D., YAN, C., WU, N., et al. An improved symbol timing error detector for QPSK signals. In *International ICST Conference on Communications and Networking in China (CHINACOM)*. Harbin (China), 2011, p. 1088–1092. DOI: 10.1109/ChinaCom.2011.6158318
- [41] SIMON, M. K., ALOUINI, M. *Digital Communication over Fading Channels*. John Wiley & Sons, 2005. ISBN: 9780471649533

## About the Authors ...

**Antonio Macilio P. de LUCENA** received the B.S. degree in Electronics Engineering from Technological Institute of Aeronautics (ITA), São José dos Campos, São Paulo, Brazil, in 1980, the M.S. degree in Space Telecommunications and Electronics from National Institute for Space Research (INPE), São José dos Campos, São Paulo, Brazil, in 1986, and the Doctor degree in Teleinformatics Engineering from Federal University of Ceara (UFC), Fortaleza, Ceará, Brazil, in 2006. He is with INPE since 1983 where he has been involved in various projects in the areas of satellite communications, electronics, and radio-astronomy. Since 2007, he is also professor of Fortaleza University (UNIFOR), Fortaleza, Ceará, Brazil. His present research interests include modulations, space communications, signal processing, and communication theory.

**Francisco A. Tavares F. da SILVA** received the B.S. in Electrical and Electronic Engineering from Federal University of Campina Grande, Campina Grande, Paraíba, Brazil, in 1986, the M.Sc. in Electronic and Computer Engineering from Aeronautics Institute of Technology, São José dos Campos, São Paulo, Brazil, in 1993 and the D.Sc. degree from National Institute for Space Research (INPE) São José dos Campos-SP, Brazil, in 1998. Since 1986 he has worked at INPE and currently conducts research in digital signal processing applied to near real time pattern

recognition and telecommunications using software defined electronic-systems.

**Adeildo S. da SILVA** graduated in Electrical Engineering at Federal University of Ceará (UFC) in 1997, received the M.Sc. degree in Signals and Systems for Communications from UFC in 2014. He is in Instituto Presbiteriano Mackenzie (IPM), São Paulo, working directly in CRAAM, at Eusébio, Ceará, Brazil, and his research interests include signal processing, space communication and modulations.